Supplementary Information (SI) for Reaction Chemistry & Engineering.
This journal is © The Royal Society of Chemistry 2025

Supplementary information (SI)

Christophe de Graaf[a], Jonas Cassimon[a], Attila Kovacs[a], Matthew Porters[a,b], Christophe M.L. Vande Velde[a], Philippe Nimmegeers[c,d], Ana da Cunha[d], Pieter Billen[a]

[a]*University of Antwerp, Faculty of Applied Engineering, Intelligence in Processes, Advanced Catalysts and Solvents (iPRACS), Groenenborgerlaan 171, 2020 Antwerp, Belgium.*
[b]*Triple Helix, Bluechem, Olieweg 95, 202 Antwerpen, Belgium. E-mail: info@triplehelixgroup.com*
[c]*Department of Engineering Management, Faculty of Business and Economics, University of Antwerp, Prinsstraat 13, 2000 Antwerp, Belgium.*
[d]*Flanders Make@UAntwerp, 2000 Antwerp, Belgium.*
[e]*Structural Chemistry Division, Department of Chemistry, University of Antwerp Groenenborgerlaan 171, B-2020 Antwerp, Belgium.*

S1) Calibration of the HPLC

Four PEG standards (PEG200, PEG600 and PEG1000 bought from TCI Europe and PEG400 bought from Sigma Aldrich) were calibrated for quantification via HPLC-ELSD. ELSD response is not linear in function of sample concentration, but follows a power-law function (in the form of $Peak\ area = a\ Concentration^{b}$ with *a* and *b* being constants). This power-law function can be rewritten as a linear function by taking the log of both term resulting in $Log_{10}(Peak\ area) = b\ Log_{10}(Concentration) + Log_{10}(a)$. By plotting the Log(peak area) in function of the Log(concentration), a linear relation is obtained for which a linear regression can be used as calibration curve. These calibration curves can be seen in Figure S1 with their associated functions and correlation coefficients.
The Calibration of 4,4'-MDA was done via HPLC-DAD on two wavelengths: 240 nm and 296 nm. As 240 nm is the peak absorbance of 4,4'-MDA, it is the ideal wavelength to detect low concentrations, while higher concentrations quickly reached the detection cutoff at 240 nm. For this reason, it was also calibrated at 296 nm as concentrations up to 6x higher could be measured at 296 nm compared to 240 nm. Both calibration curves are shown in Figure S2 together with their associated functions and correlation coefficients. The concentration units of all calibration curves were mass solute / total mass sample.

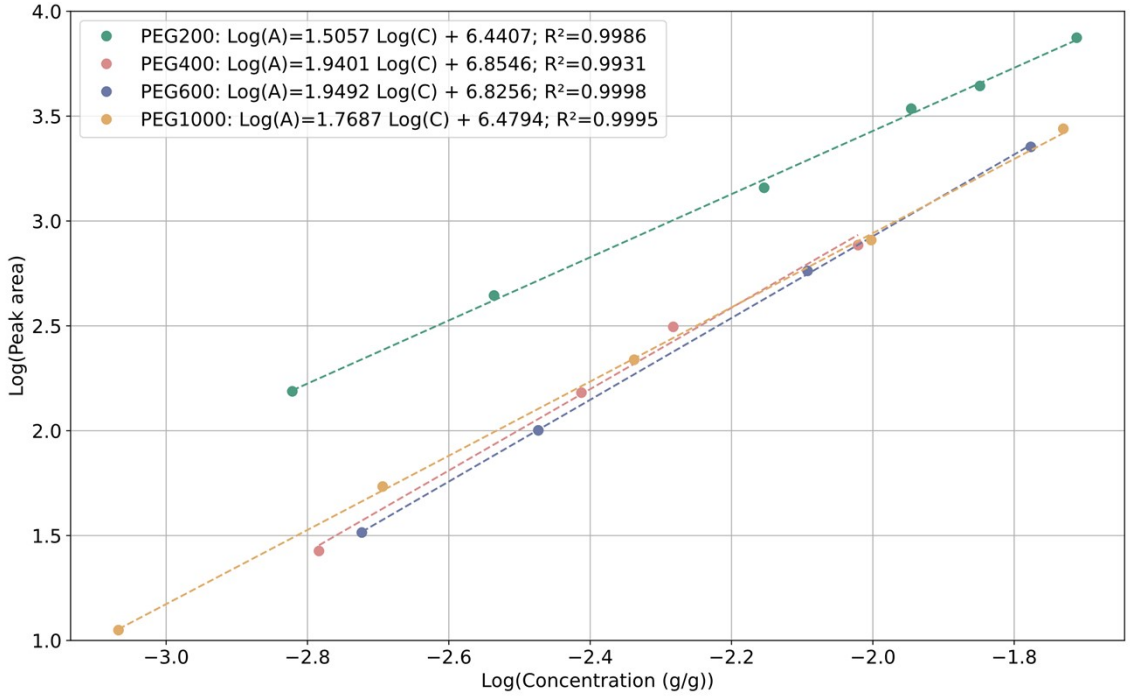

Figure S 1 Calibration curves of the four PEG standards with their functions and correlation coefficients.

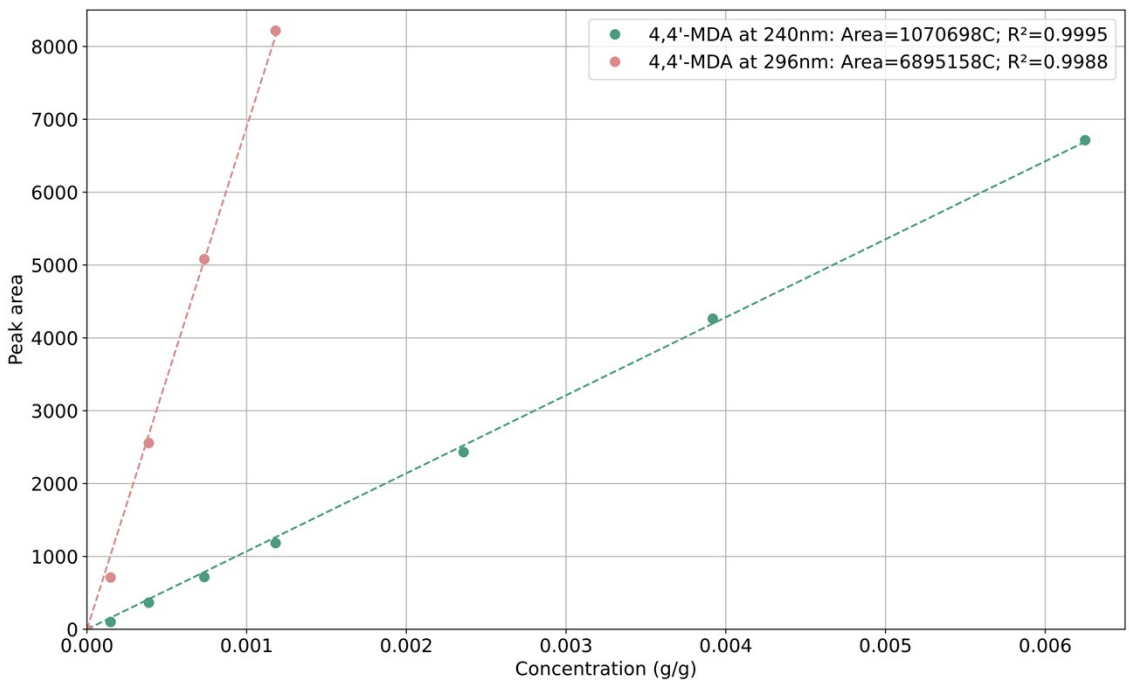

Figure S 2. Calibration curves of 4,4'-MDA at 240 nm and 296 nm for accurate quantification via HPLC-DAD at both low and higher concentrations.

S2) Mapping and parametrizing 4,4'-methyldifenyldiamine (MDA)

The study begun with the parametrization of the coarse grain model of MDA allowing for the simulations of this molecule with the others. OPLS-AA and GROMACS compatible structures and topologies were obtained via the LigParGen tool. These were used as a basis for determining the the bonded interactions for the corresponding CG model. The AA-reference simulations were performed by dis- solving 1 MDA molecule into 1692 water molecules in a box of 3.8x3.8x3.8 nm. Water, with the TIP3P forcefield, was chosen as a solvent due to the polar nature of most solvents explored in this study. The energy of the solvated box was minimized by steepest descent algorithm. The system was equilibrated first in a NVT ensemble at 298.15 K for 250 ps (Berendsen with a time constant of τ =0.1 ps) and then in a NPT ensemble at 298.15 K and 1 bar (with Berendsen barostat with P=0.5 ps and a compressibility of 4.5×10-5 bar-1). The production simulation was run in the same ensemble using the Nose-Hoover thermostat and the Parrinello-Rahman Barostat for for 50 ns with a 20 fs timestep. Then, the the chemical nature of each moiety, represented by a bead, was assessed, and an appropriate bead type was assigned. The initial structure was build using the CGbuilder tool. The same workflow was followed for the CG simulations as for the AA simulations and results were compared. The fit of the bonded parameters (such as bond lengths and reference angles) was refined by iteratively adjusting them until a satisfactory alignment between the mapped AA models and the CG models was achieved.

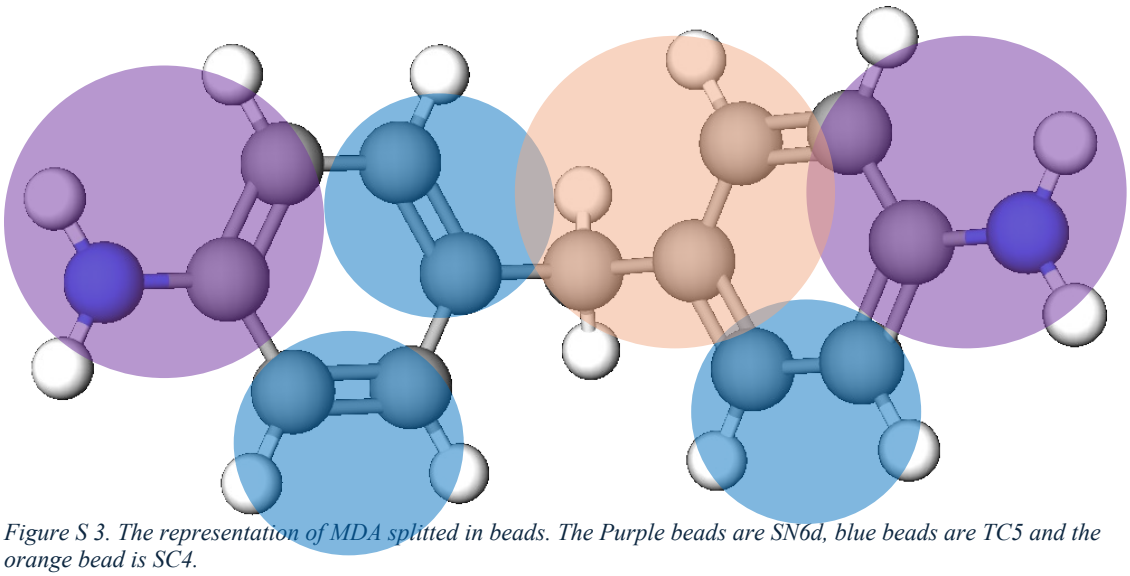

Figure S 3. The representation of MDA splitted in beads. The Purple beads are SN6d, blue beads are TC5 and the orange bead is SC4.

Bead number	Bead type
1	SN6d (purple)
2	TC5 (blue)
3	TC5 (blue)
4	SC4 (brown)
5	TC5 (blue)
6	SN6d (purple)

Table S. 1 Overview of the bead numbers assigned to the MDA molecule.

Parameter	i	j	k	Funct.	(ref) Length/angle	Force constant
Bond1	1	2	/	1	0.570	/
Bond2	1	3	/	1	0.100	/
Bond3	2	3	/	1	0.550	/
Bond4	3	4	/	1	0.230	10000

Bond 5	4	5	/	1	0.180	/
Bond 6	4	6	/	1	0.380	/
Bond 7	5	6	/	1	0.285	/
Angle 1	3	4	5	1	110.0	100.00

Table S. 2 Overview of the bonds and angle parameters with force constants and length/angle scales

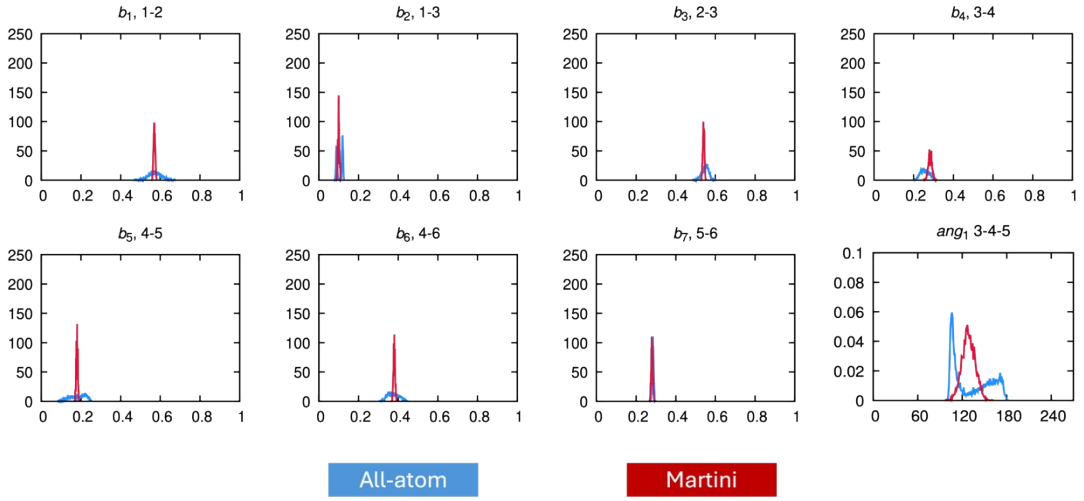

Figure S 4. CG-mapping on the all-atom simulations. Blue curves show the all-atom result and red the CG result. The bottom right figure shows the angle mapping, while the other seven plots show bond mapping.

S3) Density profiles of the different molecules

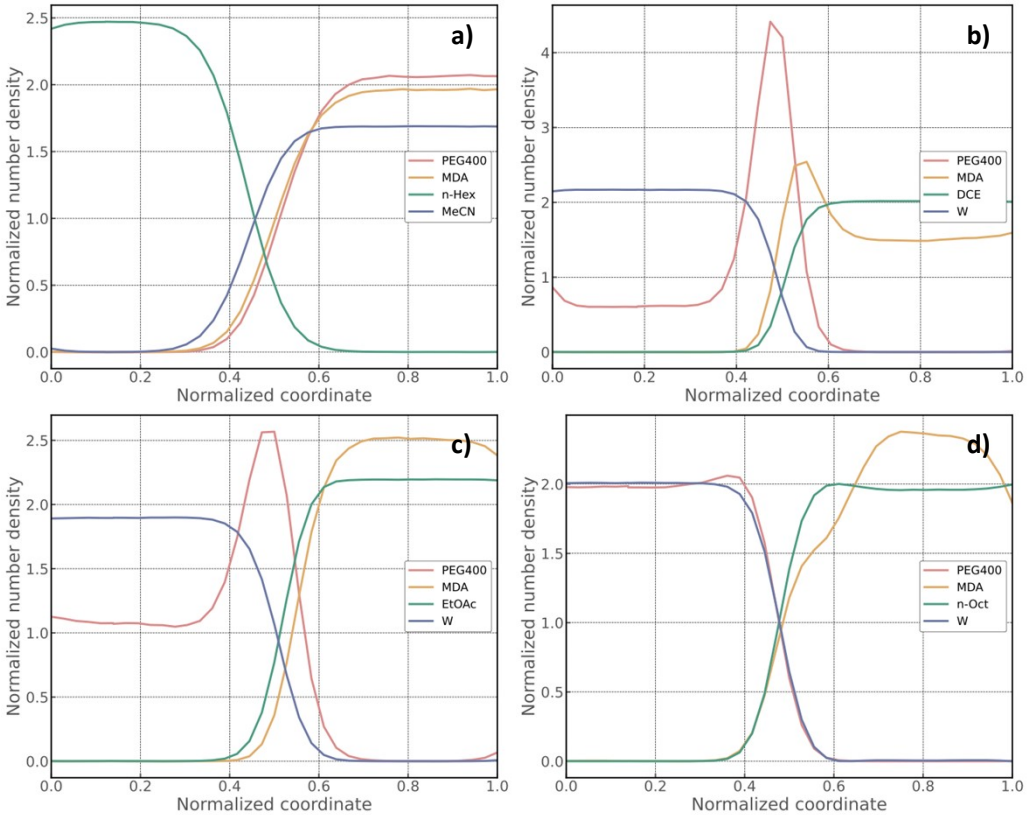

Figure S 5. Density profiles for PEG400 systems. a) MeCN/n-Hex, b) W/DCE, c) W/EtOAc, d) W/n-Oct.

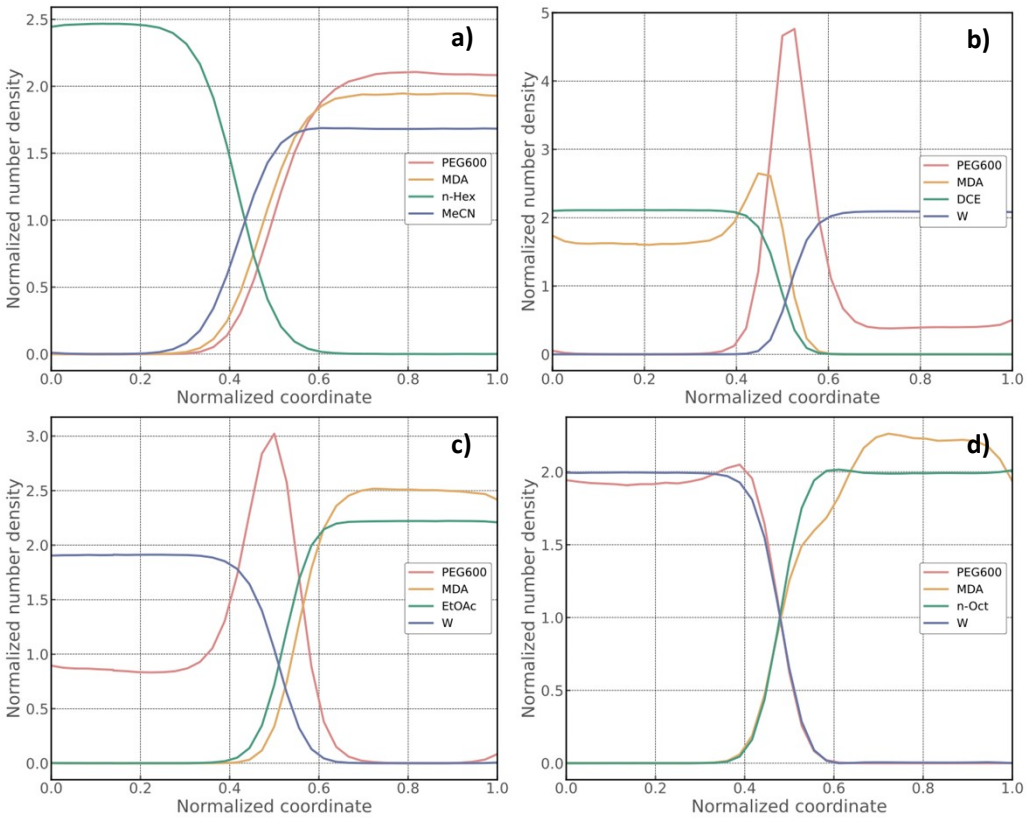

Figure S 6. Density profiles for PEG600 systems. a) MeCN/n-Hex, (b) W/DCE,c) W/EtOAc, d) W/n-Oct.

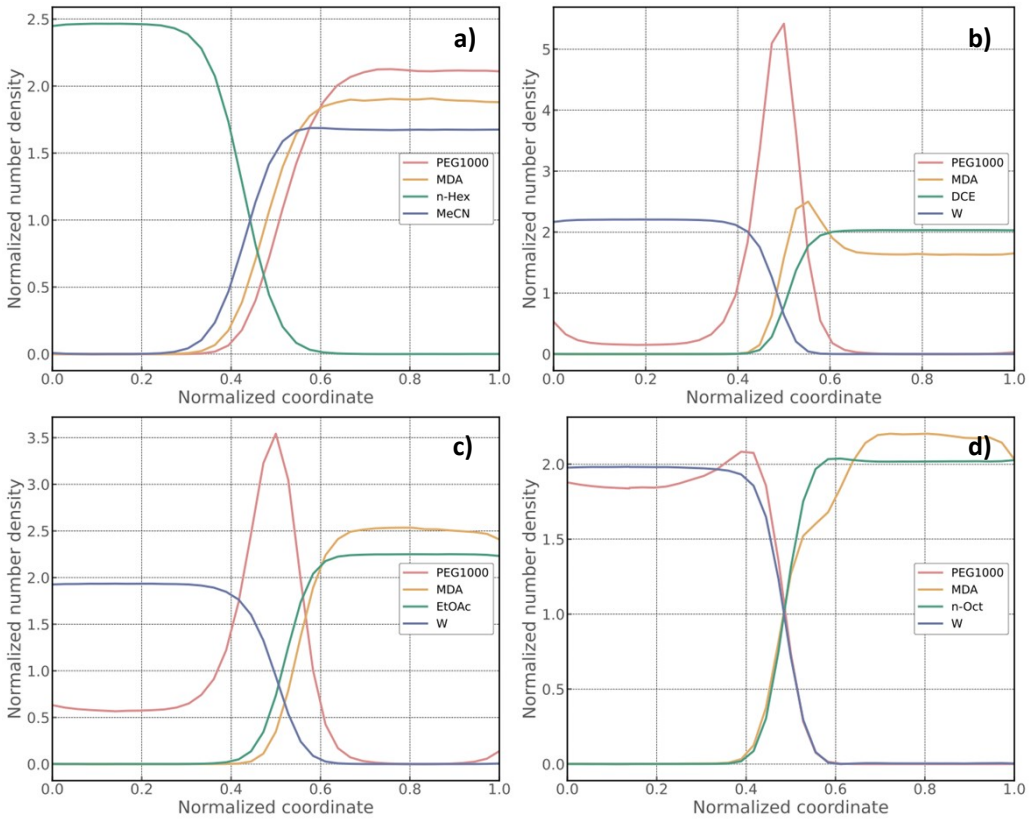

Figure S 7. Density profiles for PEG1000 systems. a) MeCN/n-Hex, b) W/DCE, c) W/EtOAc, d) W/n-Oct.

S4) Radial distribution functions

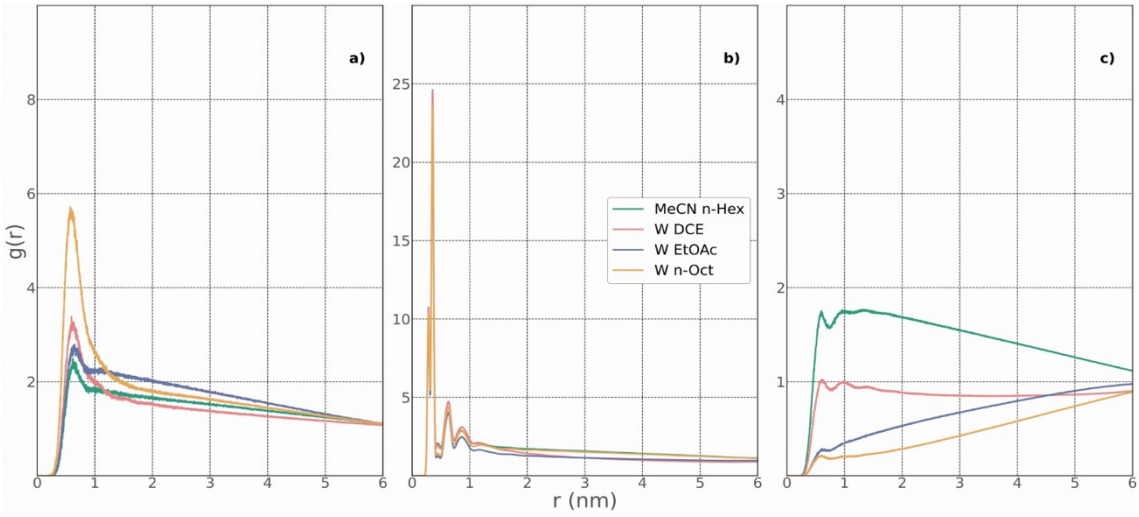

Figure S 8. RDFs of MDA-MDA COMs a), PEG400-PEG400 COMs b), PEG400-MDA COMs c) for different. RDFs were obtained from the last 500 ns of the simulation.

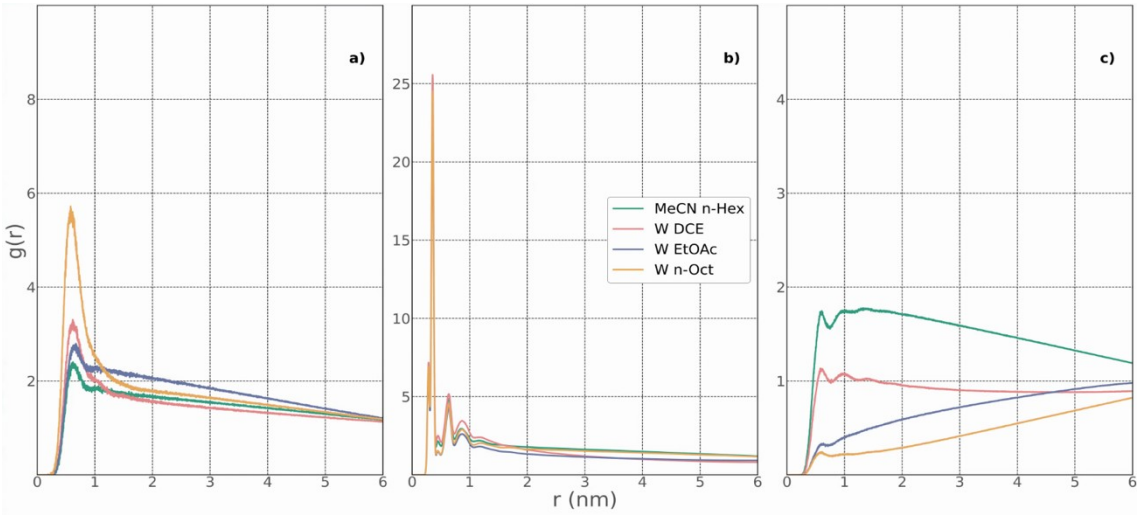

Figure S 9. RDFs of MDA-MDA COMs a), PEG600-PEG600 COMs b), PEG600-MDA COMs c) for different. RDFs were obtained from the last 500 ns of the simulation.

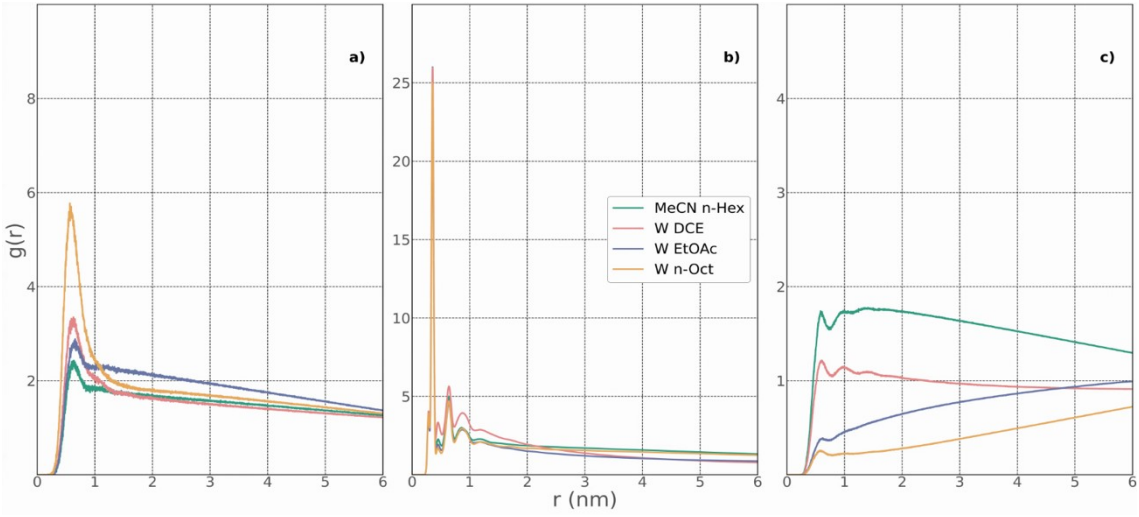

Figure S 10. RDFs of MDA-MDA COMs a), PEG1000-PEG1000 COMs(b), PEG1000-MDA COMs c) for different. RDFs were obtained from the last 500 ns of the simulation.

S5) Aggregation results

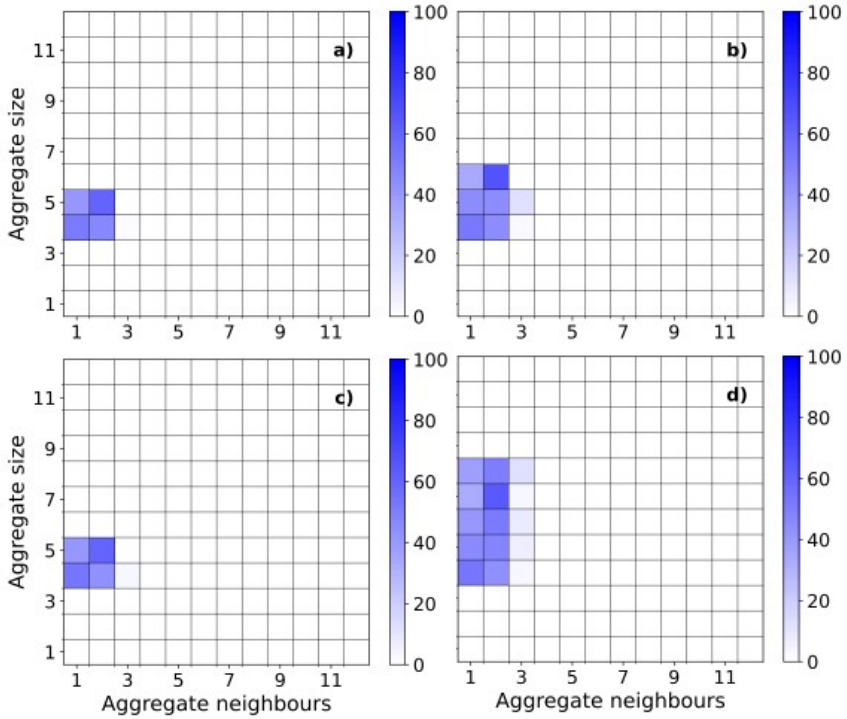

Figure S 11. Aggregate matrices of MDA-MDA COMs in PEG200-MDA system a), MeCN n-Hex b), W DCEc) W EtOAc and d) W n-Oct. For the W n-Oct, there is a clear increase in Aggregate size, with the same number of neighbours, indicating the increased interaction between the MDA molecules in the octanol phase.

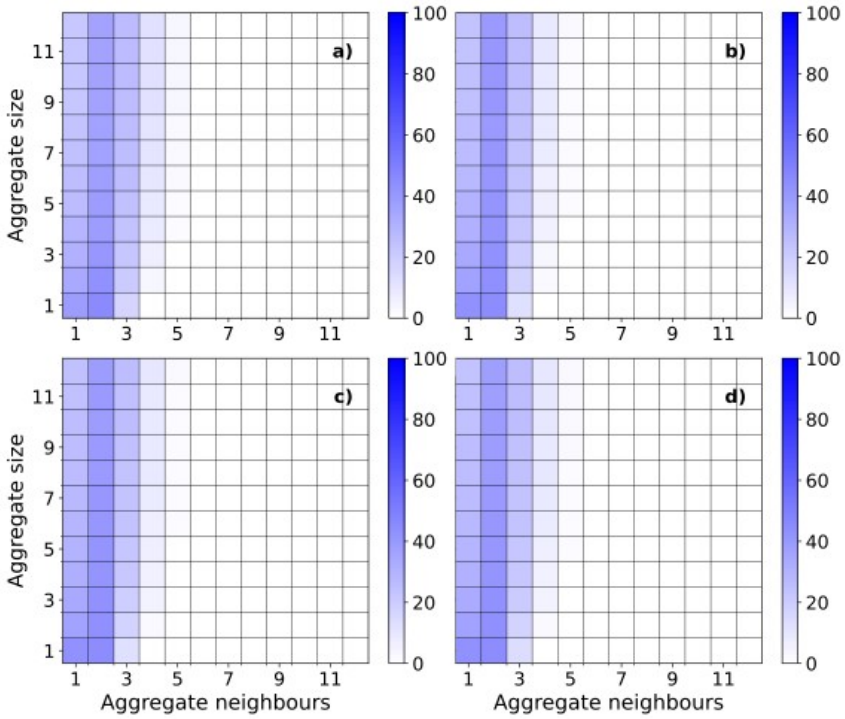

Figure S 12. Aggregate matrices of PEG200-PEG200 COMs in PEG200-MDA system a), MeCN n-Hex b), W DCE c) W EtOAc and d) W n-Oct. For the W n-Oct, there is a clear increase in Aggregate size, with the same number of neighbours, indicating the increased interaction between the MDA molecules in the octanol phase.

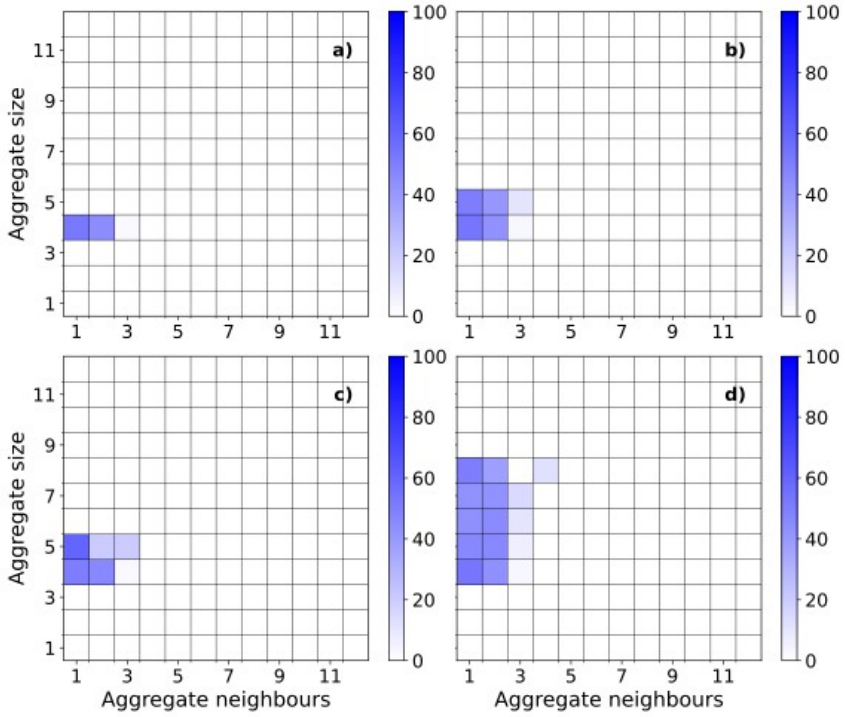

Figure S 13. Aggregate matrices of MDA-MDA COMs in PEG400-MDA system a), MeCN n-Hex b), W DCE c) W EtOAc and d) W n-Oct. For the W n-Oct, there is a clear increase in Aggregate size, with the same number of neighbours, indicating the increased interaction between the MDA molecules in the octanol phase.

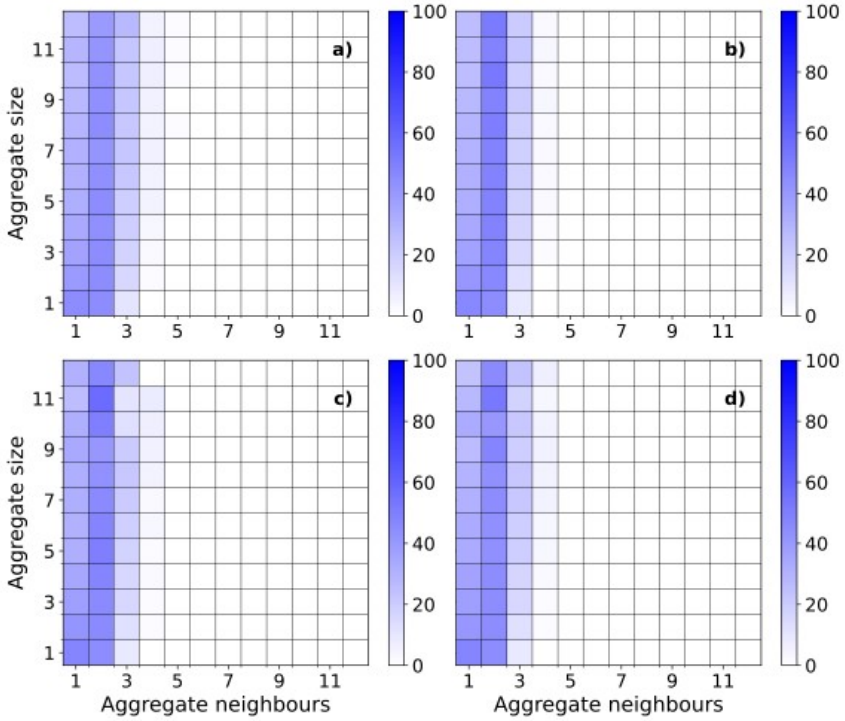

Figure S 14. Aggregate matrices of PEG400_PEG400 COMs in PEG400-MDA system a), MeCN n-Hex b), W DCE c) W EtOAc and d) W n-Oct. For the W n-Oct, there is a clear increase in Aggregate size, with the same number of neighbours, indicating the increased interaction between the MDA molecules in the octanol phase.

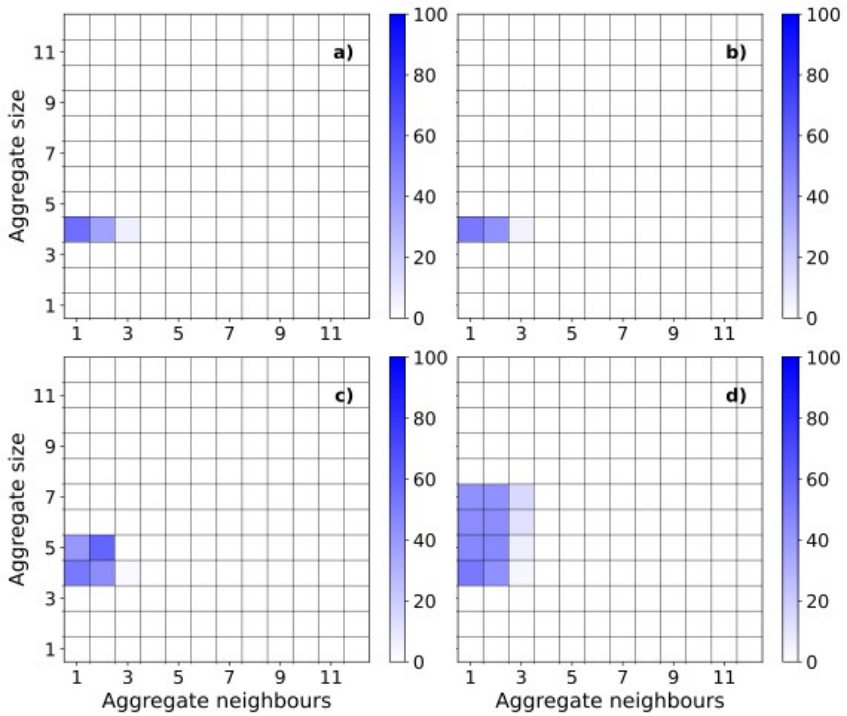

Figure S 15. Aggregate matrices of MDA-MDA COMs in PEG600-MDA system a), MeCN n-Hex b), W DCE c) W EtOAc and d) W n-Oct. For the W n-Oct, there is a clear increase in Aggregate size, with the same number of neighbours, indicating the increased interaction between the MDA molecules in the octanol phase.

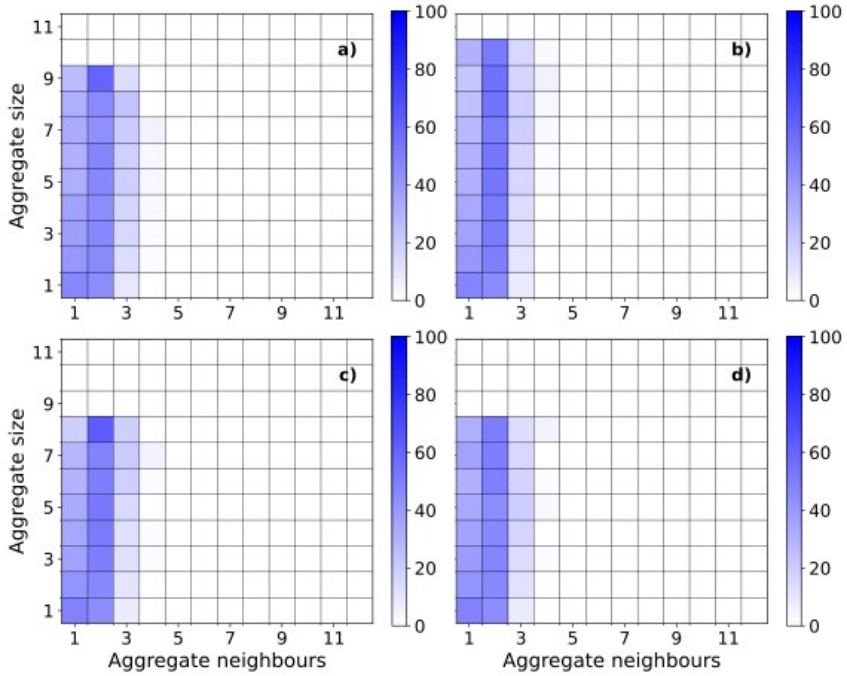

Figure S 16. Aggregate matrices of PEG600_PEG600 COMs in PEG600-MDA system a), MeCN n-Hex b), W DCE c) W EtOAc and d) W n-Oct. For the W n-Oct, there is a clear increase in Aggregate size, with the same number of neighbours, indicating the increased interaction between the MDA molecules in the octanol phase.

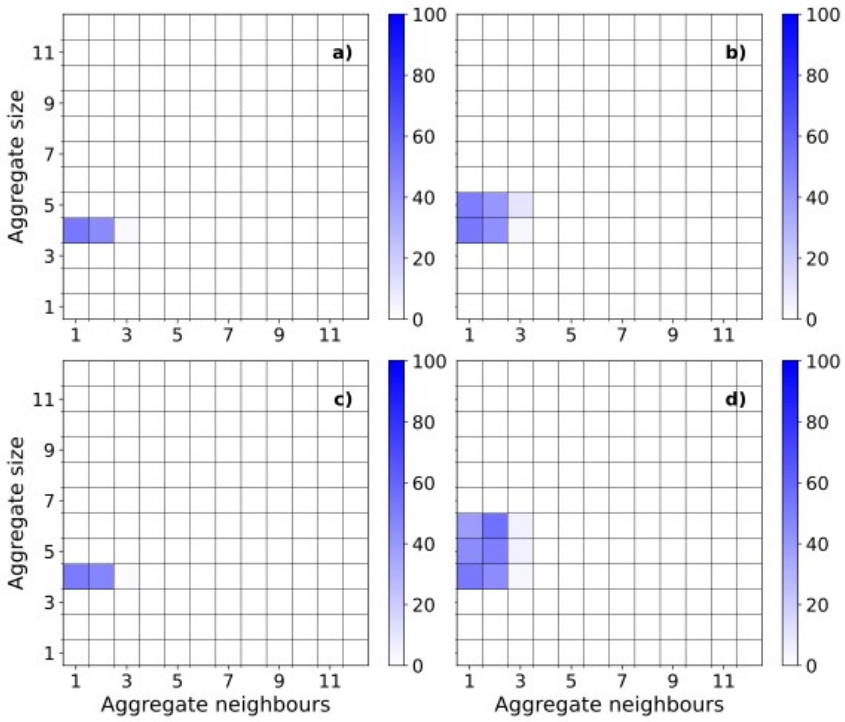

Figure S 17. Aggregate matrices of MDA-MDA COMs in PEG1000-MDA system a), MeCN n-Hex b), W DCE c) W EtOAc and d) W n-Oct. For the W n-Oct, there is a clear increase in Aggregate size, with the same number of neighbours, indicating the increased interaction between the MDA molecules in the octanol phase

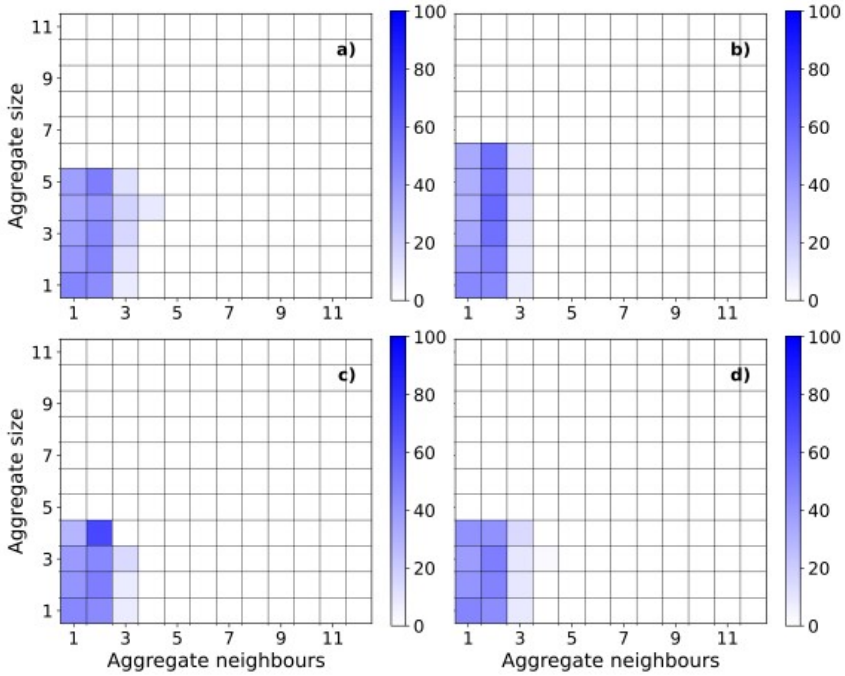

Figure S 18. Aggregate matrices of PEG1000_PEG1000 COMs in in PEG1000-MDA system a), MeCN n-Hex b), W DCE c) W EtOAc and d) W n-Oct. For the W n-Oct, there is a clear increase in Aggregate size, with the same number of neighbours, indicating the increased interaction between the MDA molecules in the octanol phase.

S6) Visual results of the separations

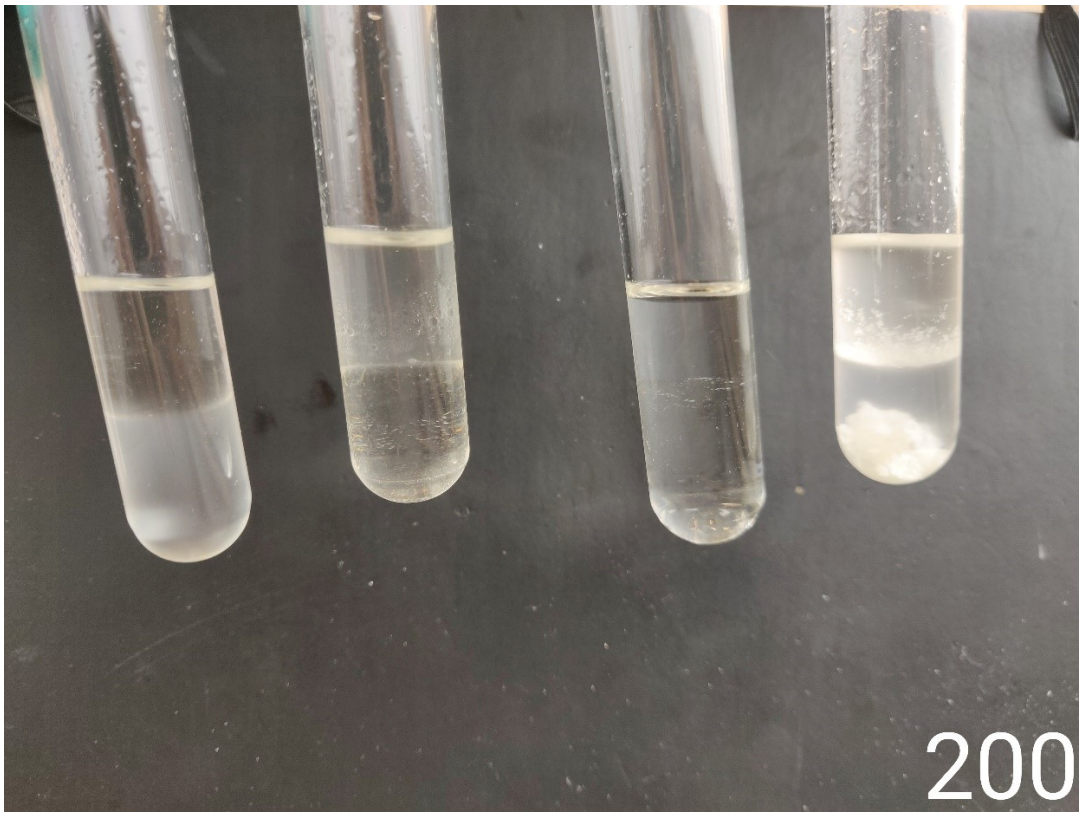

Figure S 19. Visual result of the separation of PEG200 and MDA. The mixtures are from left to right: W/EtOAc, W/DCE, MeCN/n-Hex and W/n-oct.

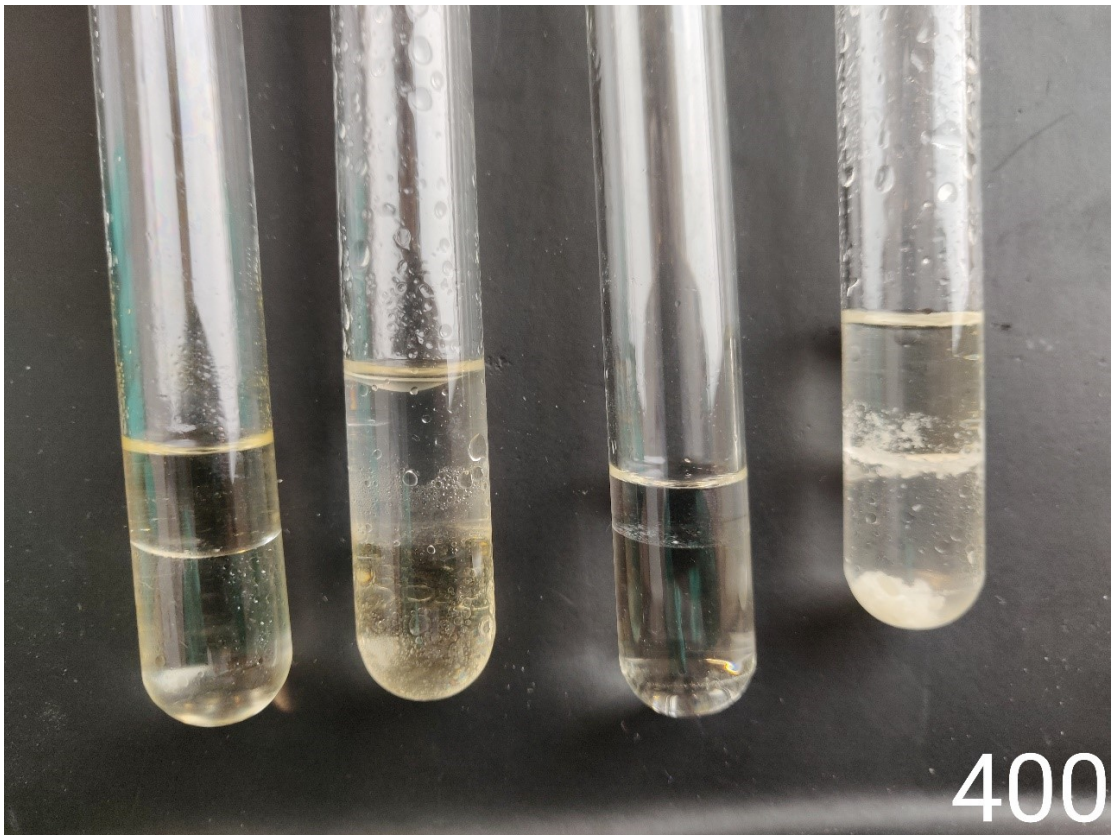

Figure S 20. Visual result of the separation of PEG400 and MDA. The mixtures are from left to right: W/EtOAc, W/DCE, Acn/n-Hex and W/n-oct.

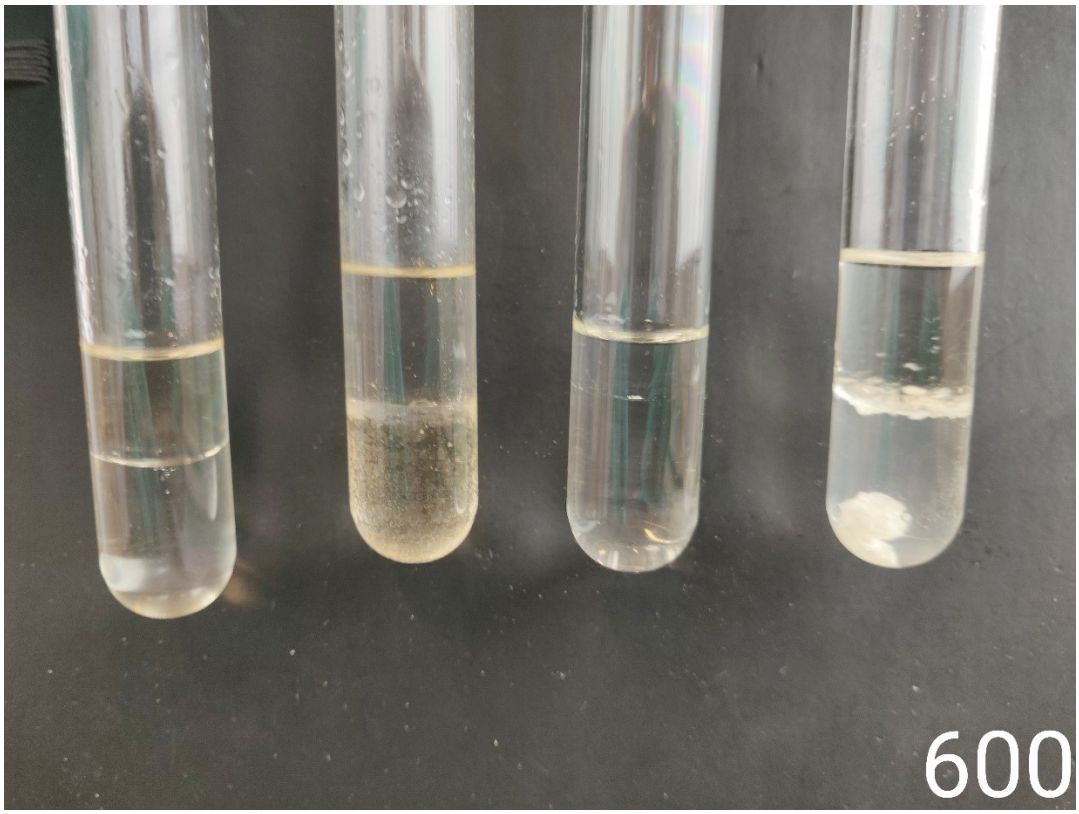

Figure S 21. Visual result of the separation of PEG600 and MDA. The mixtures are from left to right: W/EtOAc, W/DCE, MeCN/n-Hex and W/n-oct.

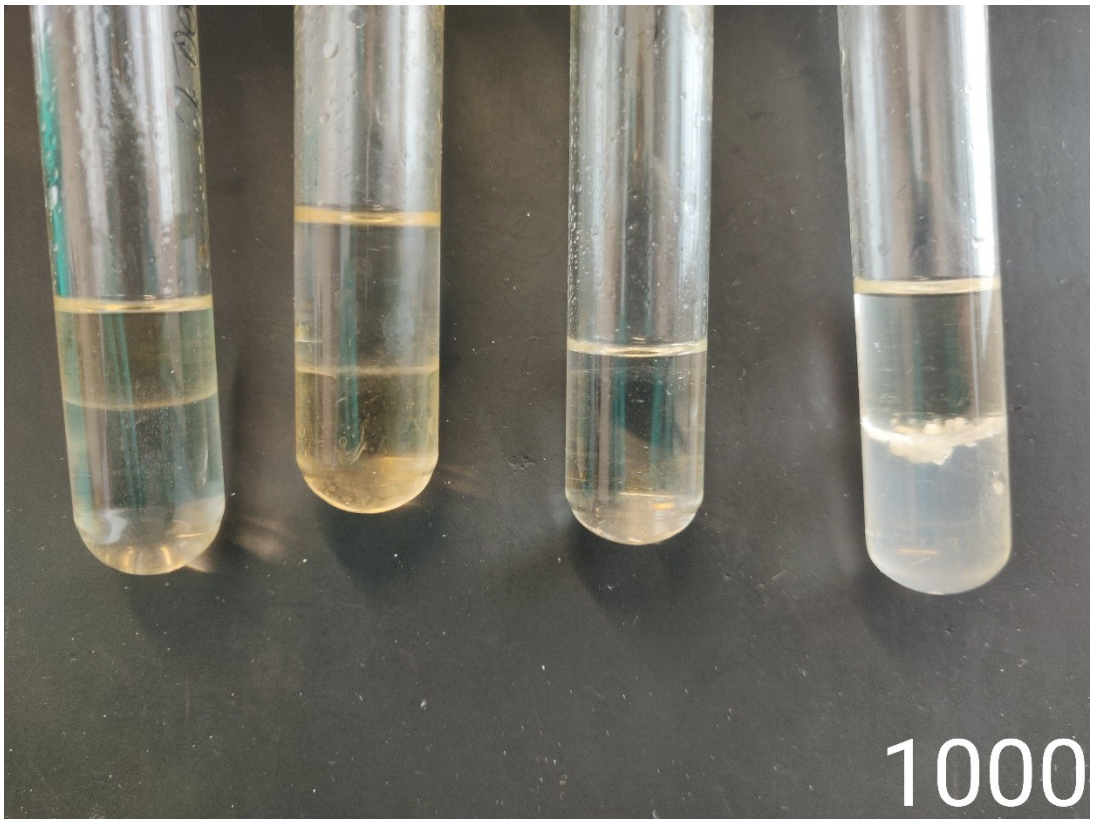

Figure S 22. Visual result of the separation of PEG1000 and MDA. The mixtures are from left to right: W/EtOAc, W/DCE, MeCN/n-Hex and W/n-oct.